Aerospace Science and Technology ••• (••••) •••–•••

Contents lists available at ScienceDirect

Aerospace Science and Technology

www.elsevier.com/locate/aescte

Fractional-order controllers optimized via heterogeneous comprehensive learning pigeon-inspired optimization for autonomous aerial refueling hose–drogue system

Yongbin Sun, Haibin Duan *, Ning Xian

State Key Laboratory of Virtual Reality Technology and Systems, Beihang University, Beijing 100083, China

ARTICLE INFO

Article history:
Received 4 February 2018
Received in revised form 20 July 2018
Accepted 23 July 2018
Available online xxxx

Keywords:
Autonomous aerial refueling (AAR)
Hose–drogue system (HDS)
Controllable drogue
Optimized fractional-order controller (FOC)
Heterogeneous comprehensive learning pigeon-inspired optimization (HCLPIO)

ABSTRACT

Dynamic modeling and control system design for the hose–drogue system (HDS) in the docking stage of autonomous aerial refueling (AAR) are investigated in this paper. The dynamics and kinematics of hose are modeled via a finite-segment multi-body method, which describes the hose–drogue assembly as a link-connected system. A controllable drogue is connected to the hose for automatically stabilizing the drogue's relative position under the influences of tanker trailing vortex, receiver bow wave, atmospheric turbulence, gust, and wind shear. Thus, a drogue position control law based on fractional-order method is designed to resist the multi-wind disturbances. Noting that it is difficult to tune the parameters of fractional-order controller (FOC), a modified pigeon-inspired optimization (PIO), the hybrid of heterogeneous comprehensive learning strategy and PIO (HCLPIO), is carried out to optimize the parameters of FOC. The simulation results show that the proposed optimized fractional-order feedback controllers effectively stabilize the controllable drogue to swing within an acceptable range.
© 2018 Elsevier Masson SAS. All rights reserved.

1. Introduction

Aerial refueling has been regarded as an effective method of increasing the endurance and range limitations of aircrafts. For manned aircrafts, if the pilots are not skilled for aerial refueling, autonomous aerial refueling (AAR) [1] would commendably assist the pilots to accomplish the task. And for unmanned aerial vehicles (UAVs), if UAVs have the ability of AAR, the autonomy of UAVs [2] would be enhanced drastically, which is a developing tendency of UAVs. Thus, AAR has drawn substantial interest from research institutions inspired by an advanced integration of UAVs into current combat missions [3,4]. Basically, three approaches are practiced for aerial refueling: the boom-receptacle refueling (BRR) [5,6], which the tanker extends the retractable boom to the fuel receptacle of receiver; the probe-and-drogue refueling (PDR) [5,6], which the tanker drags a flexible hose with a drogue and the receiver aims at inserting the probe into the drogue; the boom drogue adapter units refueling [6,7], which is the combination of the above two refueling approaches by attaching the drogue adapter units to the boom. Compared to the other two approaches, PDR outstands in certain aspects: in the processes of PDR, the receiver need not hold a strict relative position to the tanker and multiple receivers can be simultaneously refueled by a tanker equipped refueling pods. Besides, PDR is the only approach for helicopter refueling.

However, the hose–drogue assembly suffers complicated multi-wind disturbances in the processes of PDR. There always has atmospheric turbulence, gust, and wind shear in the refueling scene. Besides, the tanker and receiver respectively generate the trailing vortex and bow wave, which have different intensity concerned with the relative position of tanker and receiver. The composite multi-wind disturbances induce the hose–drogue assembly swinging dramatically, which is adverse for the accurate docking. Hence an active-control method is essential for stabilizing the drogue to swing within an acceptable range for easy and secure refueling.

To further investigate the AAR accurate docking technique, many research institutions and scholars have implemented substantial experiments and modeling analysis for the hose–drogue system (HDS). NASA Dryden Flight Research Center [8,9] gathered abundant aerodynamic data by flight tests and wind tunnel, which is obliged for modeling the dynamics of HDS. Besides, the Boeing Company [10] presented a wing-pod refueling hose model to describe the dynamic characteristics of the hose. Zhu and Meguid [11] investigated the dynamic behavior and stability of the HDS model via the finite element method with an accurate and computationally efficient curved beam element. Moreover, Ro et al. [12] modeled the dynamics of the hose–paradrogue assembly via a finite-segment approach and studied the dynamic charac-

* Corresponding author.
E-mail address: hbduan@buaa.edu.cn (H. Duan).

https://doi.org/10.1016/j.ast.2018.07.034
1270-9638/© 2018 Elsevier Masson SAS. All rights reserved.

UNCORRECTED PROOF

teristics of paradrogue assembly resulting from the atmospheric turbulence and tanker maneuver. Williamson et al. [13] developed a pendulum-based hose model combined with the model of aerodynamic drogue, which could be automatically controlled and stabilized using drogue canopy manipulation under the influences of multi-wind disturbances. Wang et al. [14] investigated the dynamic modeling of the variable-length hose–drogue system and designed a sliding mode backstepping controller for hose whipping phenomenon. As mentioned above, although the analysis and models present the dynamics of HDS, the effective active-control method for hose–drogue assembly should be exploited to stabilize the drogue's relative position in the presence of composite multi-wind disturbances.

The existing literatures mostly design the HDS controller with proportion–integration–differentiation (PID) [15]. Though the form and physical meaning of PID are explicit, the control effect would be influenced by many existing factors. The insufficient stability of PID controller for controllable drogue's position could be caused by the atmospheric turbulence and wind shear during the docking coupling. Another method known as linear quadratic regulator (LQR) [16,17] theory is also adopted for controller design. However, the dynamic model of hose–drogue assembly is nonlinear, and many feedback control states could not be measured. Thus, in this paper, fractional-order control theory [18,19] is proposed to design the fractional-order PID (FOPID) controllers for controllable drogue, which stabilizes the three-dimensional position of drogue with accessible control states regardless of linear or nonlinear HDS model. Nevertheless, the integral and derivative orders λ, μ are introduced into FOPID controller so that the difficulty of parameter tuning is rapidly enhanced due to the five-dimensional parameter $k_P, k_I, k_D, \lambda, \mu$. The inappropriate parameters could generate non-optimal system performance, so much so that induce the dramatical swing or divergence of drogue's position. Hence we adopt the modified evolutionary algorithm to optimize the capability of FOPID controllers for HDS and reduce the workload of designers.

Evolutionary algorithms (EAs), including genetic algorithm (GA) [20], particle swarm optimization (PSO) [21], artificial bee colony optimization (ABC) [22], and so on, have gathered considerable attention from optimization communities and have been successfully applied to a wide range of scientific research problems [23–25]. Pigeon-inspired optimization (PIO), a novel swarm intelligence optimization algorithm, was firstly proposed for path planning by Duan et al. [26]. For further applications of PIO, Li and Duan [27] accomplished the target detection task for UAVs, and Zhang et al. [28] solved the optimal formation reconfiguration problems of multiple orbital spacecrafts. Besides, Sushnigdha et al. [29] utilized the PIO to design a constrained entry trajectory of re-entry vehicles. Moreover, Zhao et al. [30] applied the PIO to generate the constrained gliding trajectory for hypersonic gliding vehicles. In this paper, to enhance the swarm populations' diversity of PIO, heterogeneous comprehensive learning (HCL) [31] strategy would be incorporated into PIO (HCLPIO), whose swarm populations are divided into two subpopulations for exploitation and exploration.

In this paper, the link-connected dynamic model is created for the HDS to describe the system's flexibility. The multi-wind disturbances consist of tanker trailing vortex, receiver bow wave, atmospheric turbulence, gust, and wind shear for simulating the real scene of AAR. Besides, the FOPID controllers optimized by HCLPIO are adopted to stabilize the drogue's relative position in the presence of multi-wind disturbances, which would make a significant impact on the success of AAR docking.

The remainder of this paper is organized as follows. The models of the HDS and multi-wind disturbances are described in Section 2. Then Section 3 specifies the heterogeneous comprehensive learning PIO algorithm. In Section 4, the optimized fractional-order feedback controllers are designed for stabilizing the drogue's relative position. Conclusions are contained in the final section.

2. Hose–drogue system and multi-wind disturbances environment

2.1. HDS components and coordinate system definition

The HDS contains three components: the hose, the controllable drogue, and the sensors. The hose–drogue assembly is described as a link-connected system based on the finite-segment multi-body method. In this way, the hose is divided into a certain number of links connected with frictionless joints where the aerodynamic forces and mass are concentrated according to the lumped parameter method. The controllable drogue (based on the work in [13]) is regarded as a mass point, and its aerodynamic forces could be controlled via changing the opening angles of actuators. Thus, the active-control aerodynamic forces are generated by the controllable drogue to resist the multi-wind disturbances. To simplify the model of HDS, the twist, elasticity, and damping are ignored. The hose–drogue assembly configuration and coordinate system definition are illustrated in Fig. 1.

As shown in Fig. 1, the dynamic model of the hose–drogue assembly is derived in the traction point coordinate system $O_dX_dY_dZ_d$, whose x, y, z-axes are parallel to the tanker's trajectory coordinate $O_pX_pY_pZ_p$. The inertial reference coordinate system is described as $O_gX_gY_gZ_g$. The state angles of the k-th link $\boldsymbol{d}_k$ are presented as the angles $\vartheta_{k1}, \vartheta_{k2}$ respectively relative to the planes $O_dX_dY_d$ and $O_dX_dZ_d$. The forces acting on the lumped mass k consist of hose tensions $\boldsymbol{T}_{k-1}, \boldsymbol{T}_k$, hose equivalent restoring force $\boldsymbol{R}_k$ [39], and resultant external force (the resultant force of gravity and aerodynamic forces). The controllable actuators on the drogue locate at the starboard brace (actuator 1), the port-side brace (actuator 3), the upper brace (actuator 2) aligned with the vertical, and the upper brace (actuator 4) aligned with the vertical.

2.2. Model of the HDS

The hose–drogue assembly is described as a link-connected system modeled via a finite-segment multi-body method [12,14]. To stabilize the drogue's relative position with multi-wind disturbances, the external forces of controllable drogue should be focused on.

The resultant external force $\boldsymbol{Q}_{dro}$ of controllable drogue can be expressed as [12]

$$\boldsymbol{Q}_{dro} = \left(\frac{m_N}{2} + m_{dro}\right)\boldsymbol{g} + \frac{\boldsymbol{D}_N}{2} + \boldsymbol{D}_{dro} \tag{1}$$

where m_N, m_{dro} respectively denote the mass of the hose's N-th link and the drogue; $\boldsymbol{D}_N$ is the aerodynamic force of the hose's N-th link, which can be calculated as presented in [12, 14]; $\boldsymbol{D}_{dro}$ denotes the drag force of drogue. Besides the conventional drag force of drogue, the real active-control aerodynamic force $\boldsymbol{F}'_D$ is merged to $\boldsymbol{D}_{dro}$. As shown in Fig. 1, the four cruciform actuators [13] are controlled to change the opening angles $u_{act1}, u_{act2}, u_{act3}, u_{act4}$ of drogue's struct-braces (i.e., the red lines shown in Fig. 1). Thus, the controllable drogue can change its own drag force equivalent to generate the additional active-control aerodynamic forces for reducing the range of motion of the drogue's position. Specifically, according to the wind-tunnel test results [13], if decrease u_{act1} and increase u_{act3}, the drogue would generate a positive lateral force, and if decrease u_{act2} and increase u_{act4}, a positive vertical force would be generated. Therefore, $\boldsymbol{D}_{dro}$ can be calculated as

UNCORRECTED PROOF

Please cite this article in press as: Y. Sun et al., Fractional-order controllers optimized via heterogeneous comprehensive learning pigeon-inspired optimization for autonomous aerial refueling hose–drogue system, Aerosp. Sci. Technol. (2018), https://doi.org/10.1016/j.ast.2018.07.034

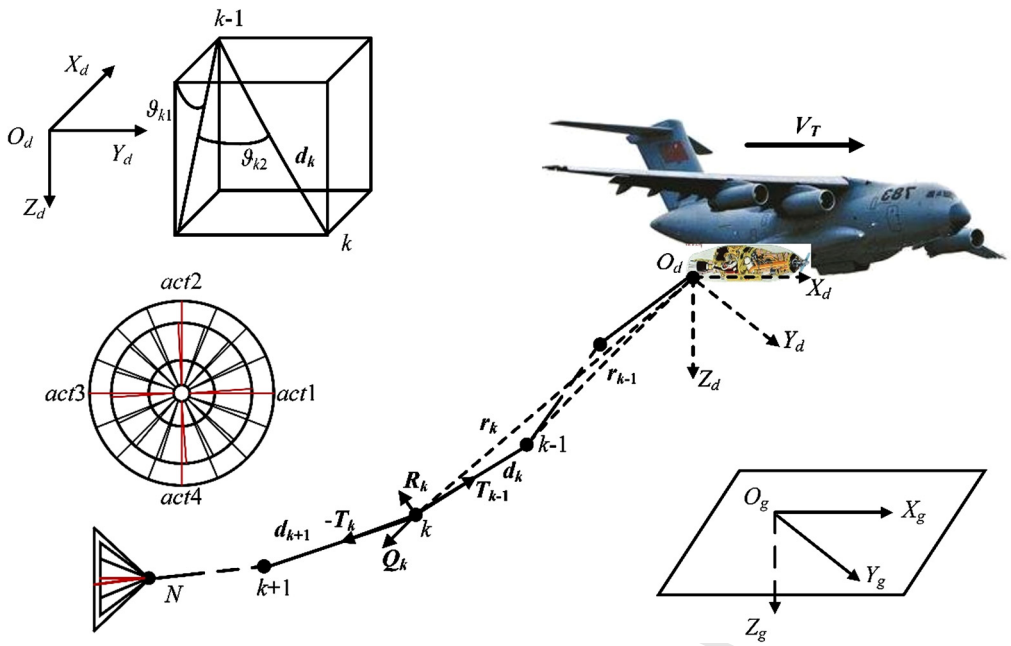

Fig. 1. Hose–drogue assembly configuration and coordinate system definition. (For interpretation of the colors in the figure(s), the reader is referred to the web version of this article.)

$$\boldsymbol{D}_{dro} = -\frac{1}{2}\rho\|\boldsymbol{V}_{N,air}\|\left(\frac{\pi d_{dro}^2}{4}\right)c_{dro}\boldsymbol{V}_{N,air} + \boldsymbol{F}'_D \tag{2}$$

where ρ is the local air density; $\boldsymbol{V}_{N,air} = \boldsymbol{V}_N - \boldsymbol{V}_w$, $\boldsymbol{V}_N$ represents the velocity of the hose's N-th lumped mass, and $\boldsymbol{V}_w$ is the local wind velocity caused by the multi-wind disturbances; c_{dro} denotes the drag force coefficient of drogue; d_{dro} is the diameter of drogue. The expected active-control aerodynamic force for the design of controllers is presented as $\boldsymbol{F}_D = [0\ F_s\ F_v]^T$, in which F_s, F_v are respectively the expected lateral and vertical forces generated by changing the opening angles of canopy. Considering the horizontal aerodynamic force of drogue would be changed in actual situations, the real active-control aerodynamic forces $\boldsymbol{F}'_D$, $\boldsymbol{F}'_D = [F'_h\ F'_s\ F'_v]^T$, is computed as [13]

$$\boldsymbol{F}'_D = \frac{1}{2}\rho\|\boldsymbol{V}_{N,air}\|^2\boldsymbol{C}_u(\boldsymbol{u}_{act} - \boldsymbol{u}_0) \tag{3}$$

where $\boldsymbol{C}_u$ represents the opening angular coefficient for active control; $\boldsymbol{u}_{act}$ is the opening angles of actuators; $\boldsymbol{u}_0$ is the opening angles of the drogue's equilibrium state. Considering the roll angle of drogue is tiny, F'_s, F'_v are respectively generated by the horizontal actuators (i.e., *act*1 and *act*3 in Fig. 1) and the vertical actuators (i.e., *act*2 and *act*4 in Fig. 1). If the horizontal or vertical actuators change the opposite angle, F'_h is approximate to zero since the opposite effect of the actuators in a line.

2.3. Multi-wind disturbances environment

The states of the hose–drogue assembly can be easily affected by the multi-wind disturbances, including the tanker trailing vortex, receiver bow wave, atmospheric turbulence, gust, and wind shear.

2.3.1. Tanker trailing vortex

Due to the high precision and easy implementation for simulation, the tanker trailing vortex is built as Hallock–Burnham model [32] which is experimented via flight tests. The wind velocity of Hallock–Burnham model is expressed as $[V_{vorx}\ V_{vory}\ V_{vorz}]$, where the component V_{vorx} is approximate to zero according to the property of this model. Besides, the components V_{vory}, V_{vorz} are computed as

$$V_{vory} = \frac{\Gamma_0}{2\pi}\left[\frac{z_{rel}}{(y_{rel} - \pi b_T/8)^2 + r_c^2 + z_{rel}^2} - \frac{z_{rel}}{(y_{rel} + \pi b_T/8)^2 + r_c^2 + z_{rel}^2}\right] \tag{4}$$

$$V_{vorz} = \frac{\Gamma_0}{2\pi}\left[\frac{y_{rel} + \pi b_T/8}{(y_{rel} + \pi b_T/8)^2 + r_c^2 + z_{rel}^2} - \frac{y_{rel} - \pi b_T/8}{(y_{rel} - \pi b_T/8)^2 + r_c^2 + z_{rel}^2}\right] \tag{5}$$

where $(x_{rel}\ y_{rel}\ z_{rel})$ denotes the coordinates relative to the trailing vortex coordinate system $O_vX_vY_vZ_v$ whose Y_v passes through the center of both trailing vortexes at wing trailing edge pointed to the right wingtip, O_v locates at the middle of the center of both trailing vortexes along Y_v, and X_v, Z_v are parallel to the tanker-body coordinate system; Γ_0 is the initial intensity of trailing vortex, $\Gamma_0 = 4G_T/(\pi\rho V_T b_T)$, in which G_T, V_T are respectively the gravity and velocity of tanker, $G_T = m_T g$; b_T is the tanker's span; r_c represents the radius of trailing vortex.

Noting that the trailing vortex tends to move down and the trailing vortex coordinate system $O_vX_vY_vZ_v$ has an offset $(d_x\ 0\ d_z)$ relative to the tanker-body coordinate system, thus the wind velocity of tanker trailing vortex should be improved. Correspondingly, the wind velocity components V'_{vory}, V'_{vorz} of the improved Hallock–Burnham model are expressed as

$$V'_{vory} = \frac{\Gamma_0}{2\pi}\left[\frac{z'_{rel}}{(y'_{rel} - \pi b_T/8)^2 + r_c'^2 + z_{rel}'^2} - \frac{z'_{rel}}{(y'_{rel} + \pi b_T/8)^2 + r_c'^2 + z_{rel}'^2}\right] \tag{6}$$

$$V'_{vorz} = \frac{\Gamma_0}{2\pi}\left[\frac{y'_{rel} + \pi b_T/8}{(y'_{rel} + \pi b_T/8)^2 + r_c'^2 + z_{rel}'^2} - \frac{y'_{rel} - \pi b_T/8}{(y'_{rel} - \pi b_T/8)^2 + r_c'^2 + z_{rel}'^2}\right] \tag{7}$$

UNCORRECTED PROOF

Please cite this article in press as: Y. Sun et al., Fractional-order controllers optimized via heterogeneous comprehensive learning pigeon-inspired optimization for autonomous aerial refueling hose–drogue system, Aerosp. Sci. Technol. (2018), https://doi.org/10.1016/j.ast.2018.07.034

where $x'_{rel} = x^T_{rel} + d_x$, $y'_{rel} = y^T_{rel}$, $z'_{rel} = z^T_{rel} + d_z + V_{mz}(x'_{rel}/V_T)$, in which $(x^T_{rel}\ y^T_{rel}\ z^T_{rel})$ is the coordinates of one point in the trailing vortex field relative to the tanker-body coordinate system and V_{mz} is the velocity of the trailing vortex moving down, $V_{mz} = 2\Gamma_0/(\pi^2 b_T)$; r'_c denotes the improved radius of trailing vortex, $r'_c = 0.5\sqrt{-(x_{rel} + d_x)/V_T}$.

2.3.2. Receiver bow wave

The dynamic motion of drogue caused by the approaching receiver has an adverse influence on a successful refueling docking. The drogue tends to move away from the receiver as it approaches, typically to the outward and upward directions since the effect of bow wave up-wash. Rankine half body model [33] is implemented to describe the bow wave, which obtains its wind velocity acting on the lumped mass. The Rankine half body model is specified as the superposition of averaged flow and point source flow. The streamline equation of bow wave is expressed as Eq. (8) in the polar coordinate system.

$$\psi = Ur\sin\theta + \frac{Q_b}{2\pi}\theta \tag{8}$$

where U is the velocity of averaged flow; Q_b denotes the intensity of point source flow, $Q_b = 2\pi U b_n$, in which b_n is the distance from the beginning of fuselage to the center of point source flow, $b_n = h_{nose}/\pi$, h_{nose} is the maximum radius of fuselage in the width direction; r represents the polar radius; θ is the polar angle.

The radial velocity v_r and circumferential velocity v_θ of bow wave relative to the polar coordinate system can be computed as

$$v_r = \frac{1}{r}\frac{\partial\psi}{\partial\theta} = U\cos\theta + \frac{Q_b}{2\pi r} \tag{9}$$

$$v_\theta = -\frac{\partial\psi}{\partial r} = -U\sin\theta \tag{10}$$

Further, the wind velocity $[v_{bowx}\ v_{bowy}\ v_{bowz}]$ of bow wave relative to the three-dimensional cartesian coordinate system is expressed as

$$\begin{aligned} v_{bowx} &= v_r\cos\theta - v_\theta\sin\theta \\ v_{bowy} &= (v_r\sin\theta + v_\theta\cos\theta)\frac{y_b^2}{\sqrt{y_b^2 + z_b^2}} \\ v_{bowz} &= (v_r\sin\theta + v_\theta\cos\theta)\frac{z_b^2}{\sqrt{y_b^2 + z_b^2}} \end{aligned} \tag{11}$$

where $(x_b\ y_b\ z_b)$ are the coordinates relative to the bow wave coordinate system $O_bX_bY_bZ_b$ whose origin O_b locates at the center of point source flow, and x, y, z-axes are parallel to the receiver-body coordinate system.

2.3.3. Other wind disturbances

Other wind disturbances exist in the AAR flowfield environment including atmospheric turbulence, gust, and wind shear. The atmospheric turbulence can induce high-frequency irregular position swinging of the drogue. The gust and wind shear correspondingly produce momentary position changing of the drogue.

We adopt the atmospheric turbulence model as the continuous Dryden turbulence [34], which is prescribed in MIL-F-8785C. Additionally, the gust and wind shear are implemented as a step function.

3. Heterogeneous comprehensive learning PIO algorithm

3.1. Basic PIO algorithm

Inspired by the homing pigeons, Duan and Qiao [26] firstly put forward the basic PIO algorithm, which requires personal and global optimization and local optimal information pigeon. The basic PIO algorithm contains the map and compass operator, and landmark operator according to the behaviors of homing pigeons in searching the destination. The conduction of the two operators achieves better performance in finding the individual and global best position.

(1) Map and compass operator:

In this operator, for a D-dimension search space, the i-th pigeon's position $X_i = [x_i^1, x_i^2, \ldots, x_i^D]$ and velocity $V_i = [v_i^1, v_i^2, \ldots, v_i^D]$ are updated in each iteration. The i-th pigeon's new position and velocity at the t-th iteration are calculated as follows [26]:

$$V_i(t) = V_i(t-1)\cdot e^{-Rt} + rand\cdot\big(gbest - X_i(t-1)\big) \tag{12}$$

$$X_i(t) = X_i(t-1) + V_i(t-1) \tag{13}$$

where R is the map and compass factor which reduces the velocity of evolution; $rand$ denotes a rand number, $rand \in [0, 1]$; $gbest$ is the current global best position which can be obtained by comparing all the positions of pigeons.

(2) Landmark operator:

The leading pigeons will fly directly to the destination once they are familiar with the landmarks. However, supposing other pigeons still far from the destination, they will follow the leading pigeons to land at the destination. Hence half of the pigeons will regard the center of all the pigeons as the destination which they fly directly to. Therefore, the number of pigeons $N_p(t)$ is decreased by a half in every iteration in this operator. The center of pigeons $X_c(t)$ and the position of pigeons $X_i(t)$ at the t-th iteration can be updated as [26]

$$N_p(t) = \frac{N_p(t-1)}{2} \tag{14}$$

$$X_c(t) = \frac{\sum_{Np} X_i(t)\cdot fitness(X_i(t))}{\sum fitness(X_i(t))} \tag{15}$$

$$X_i(t) = X_i(t-1) + rand\cdot\big(X_c(t) - X_i(t-1)\big) \tag{16}$$

where $fitness(\bullet)$ is the fitness function which denotes the cost of a pigeon. In this paper, to maintain the position of drogue, we can minimize the sum of squares of drogue's position errors as the fitness function.

3.2. HCLPIO algorithm

The heterogeneous comprehensive learning strategy is incorporated into pigeon-inspired optimization, abbreviated as HCLPIO, to increase the diversity of basic PIO. The swarm populations of HCLPIO are divided into two subpopulations, which can balance the capacities of exploitation and exploration to overcome the adverse mutual influence. The exploitation–subpopulation emphasizes on refining the promising solutions in the potential solution regions to obtain the optimal solution, while the exploration-subpopulation focuses on finding various potential solution regions of the entire search space. In both subpopulations of HCLPIO, the velocities of pigeons are updated using all the pigeons' *pbests* (*pbest* denotes the best position of a pigeon). Specifically, each dimension of a pigeon learns from different pigeons' *pbests* instead of the same *pbest* for all dimensions, which enhances the diversity of the swarm populations.

(1) Modified map and compass operator:

The i-th pigeon's new velocity of the exploitation–subpopulation for each dimension at the t-th iteration is calculated as

$$\begin{aligned} V_i^d(t) = V_i^d(t-1)\cdot e^{-Rt} &+ rand_i^d\cdot\big(pbest^d_{f_i(d)} - X_i^d(t-1)\big) \\ &+ rand_i^d\cdot\big(gbest^d - X_i^d(t-1)\big) \end{aligned} \tag{17}$$

UNCORRECTED PROOF

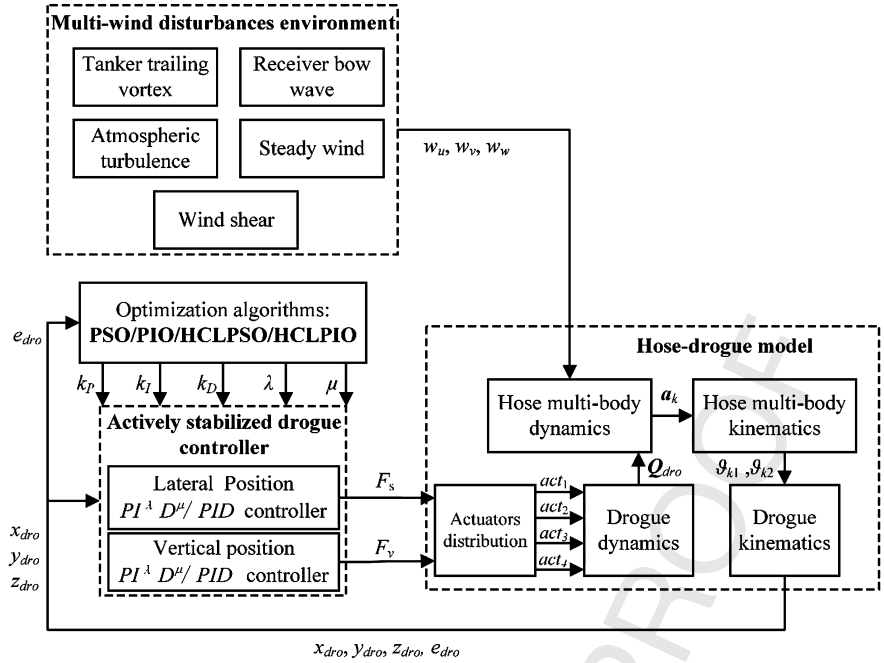

Fig. 2. Design of the optimized controllers for hose–drogue system.

where d is the number of dimension; the exemplar $f_i(d) = [f_i(1), f_i(2), \cdots, f_i(D)]$ decides whether the i-th pigeon follows its own or another's *pbest* for each dimension, which is determined according to the learning probability Pc values. The Pc_i^d value of the i-th pigeon's d-th dimension is computed as [31]

$$Pc_i^d = a_p + b_p * \frac{e^{(10(i-1)/(N_p-1))} - 1}{e^{10} - 1} \tag{18}$$

where N_p denotes the population size of pigeons; a_p, b_p are the learning probability coefficient. If $rand_i^d < Pc_i^d$, the i-th pigeon will learn from another pigeon's *pbest* for the d-th dimension. The exemplar is determined with the tournament selection procedure in which two pigeons are randomly selected from the exploitation–subpopulation and the corresponding dimension will learn from the pigeon with better fitness. Otherwise if $rand_i^d > Pc_i^d$, the d-th dimension of the i-th pigeon will learn from its own *pbest*.

The i-th pigeon's new velocity of the exploration-subpopulation for each dimension at the t-th iteration is updated as

$$V_i^d(t) = V_i^d(t-1) \cdot e^{-Rt} + rand_i^d \cdot \left(pbest_{f_i(d)}^d - X_i^d(t-1)\right) \tag{19}$$

(2) The modified landmark operator is the same as the basic landmark operator.

4. Optimized fractional-order feedback controllers

4.1. Realization of fractional-order calculus operator

Compared with the integral-order PID, the fractional-order $PI^{\lambda}D^{\mu}$ extends the order of calculus operator from integer to fraction, even complex number, which may provide better disturbance rejection performance, tracking characteristics, and robustness [35] for systems. Among all the realizations of fractional-order calculus operator s^{α}, the modified Oustaloup's method [36] can be adopted to approximate the operator for obtaining the transfer functions of controllers. The modified Oustaloup's method enhances the fitting effect of fitting frequency band endpoint by the Taylor series expansion of the basic Oustaloup's equation [37] in the fitting frequency band $[\omega_1, \omega_2]$, which is expressed as [36]

$$s^{\alpha} \approx \left(\frac{d_f\omega_2}{b_f}\right)^{\alpha} \left(\frac{d_f s^2 + b_f\omega_2 s}{d_f(1-\alpha)s^2 + b_f\omega_2 s + d_f\alpha}\right) \prod_{k=-M}^{M} \frac{s+\omega_k'}{s+\omega_k} \tag{20}$$

where α is the order of calculus operator; $2M+1$ denotes the order of fitting; $\omega_k' = (\frac{d_f\omega_1}{b_f})^{(\alpha-2k)/(2M+1)}$; $\omega_k = (\frac{b_f\omega_2}{d_f})^{(\alpha+2k)/(2M+1)}$; b_f, d_f represent the fitting coefficients.

4.2. Optimized fractional-order controllers for HDS

The proposed optimized fractional-order $PI^{\lambda}D^{\mu}$ controllers are carried out to stabilize the drogue's relative position in the presence of composite multi-wind disturbances. As depicted in Fig. 2, the simulation system contains three parts: the hose–drogue model (Section 2), the multi-wind disturbances environment (Section 2), and the optimized controllers (Section 3 and Section 4). First, design the FOPID controllers for the lateral and vertical actuators to obtain the expected aerodynamic forces F_s, F_v. Then, distribute the relevant actuators to change the opening angles. Specifically, two horizontal actuators change the opposite angles to generate the real lateral force F_s', and two vertical actuators for the real vertical force F_v'. Finally, utilize the HCLPIO algorithm to optimize the parameters of FOPID controllers, which contributes to enhance the stability and performance of the controllers.

The implementation procedures of the HCLPIO optimized fractional-order controllers for HDS can be described as follows:

Step 1: Obtain the stabilized position of the controllable drogue. Model the HDS and add the steady wind disturbance (i.e., tanker trailing vortex) to the model. Calculate the equations of hose–drogue model until the position of drogue stabilizes.

Step 2: Initialize the parameters. Initialize parameters of HCLPIO including the number of pigeons' swarm populations (N_p), the number of dimension for the problem (D), the number of exploitation–subpopulation (N_t), the number of exploration-subpopulation (N_r), and so on.

Step 3: Evaluate the fitness values of initial pigeons. Calculate the sum of squares of position errors for the controllable drogue to evaluate the initial parameters of $PI^{\lambda}D^{\mu}$ controllers.

UNCORRECTED PROOF

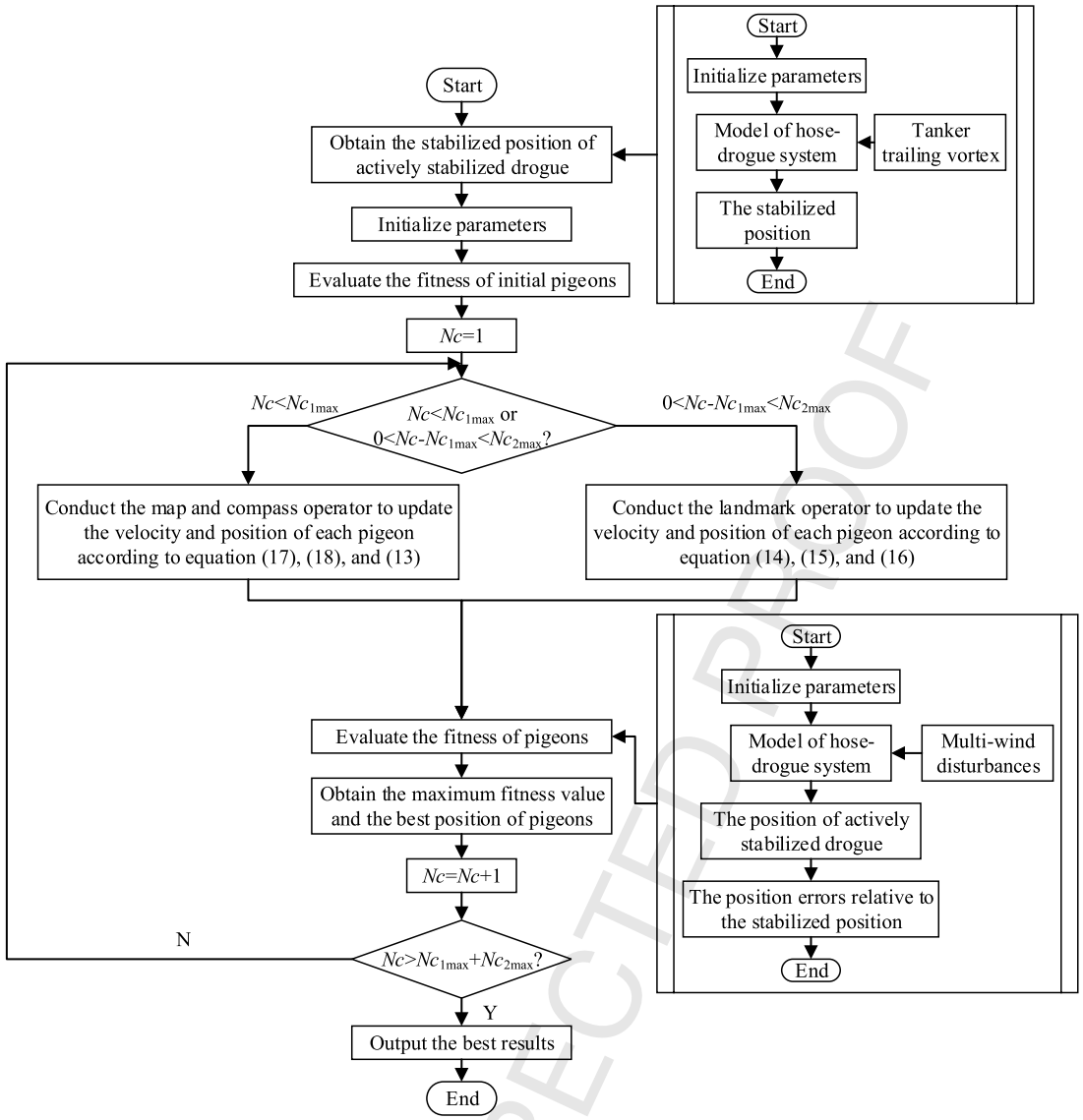

Fig. 3. Detailed flow chart of HCLPIO for the optimized fractional-order controllers.

Step 4: Conduct the selected operator to update the pigeons. If the number of iterations Nc is less than the maximum number of map and compass operator $N_{c1\max}$, then conduct the modified map and compass operator. Otherwise, perform the modified landmark operator.

Step 5: Evaluate the fitness values of pigeons. Implement the processes of HDS simulation with all the wind disturbances to obtain the drogue's position errors relative to the stabilized position, then calculate the sum of squares.

Step 6: Obtain the maximum fitness value and the best position of pigeons. According to the fitness value, select the best position of pigeons which is the optimized parameters of $PI^{\lambda}D^{\mu}$ controllers.

Step 7: Terminate if the current number of iterations Nc reaches the $Nc_{1\max} + Nc_{2\max}$, output the results. Otherwise, go to step 4.

The detailed flow of HCLPIO for the optimized fractional-order controllers is depicted in Fig. 3.

5. Simulation results and analysis

To demonstrate the validity of our proposed optimized fractional-order controllers, extensive simulations are implemented based on the dynamic model of HDS under the influence of multi-wind disturbances. The procedures of PSO and HCLPSO are implemented as described in Lynn and Suganthan's paper [31]. The equations of PSO are given in Appendix A. And the parameters (as applied in other works) of HDS [14], PSO [31], PIO [27], HCLPSO and HCLPIO are respectively presented in Table 1, Table 2, and other parameters for simulations are listed in Table 3. Here we make comparisons in two aspects: the conventional optimized PID controllers and our proposed optimized FOPID controllers for HDS; PSO, PIO, HCLPSO, and HCLPIO for FOPID controllers.

Table 1
Parameters of hose–drogue system.

Parameter	Description	Value
L	Hose total length	22.86 (m)
N	Number of links	24
m_{dro}	Mass of drogue	29.5 (kg)
d_{dro}	Diameter of drogue	0.61 (m)
c_{dro}	Drag force coefficient of drogue	0.831

Case 1. Assume that the docking stage of AAR is implemented in the light turbulence from $t = 50$ s, and the gust is acted from $t = 90$ s. Suppose the tanker makes fixed straight level flight at height

UNCORRECTED PROOF

Table 2
Parameters of PSO, PIO, HCLPSO and HCLPIO.

PSO, HCLPSO			PIO, HCLPIO		
Parameter	Description	Value	Parameter	Description	Value
N_s	Number of particles	100	N_p	Number of pigeons	100
$Nc_{\max}$	Max iteration	100	R	The map and compass factor	0.2
c_1	Self acceleration coefficient (linearly decrease from 2.5 to 0.5)	2.5–0.5	$Nc_{\max}$	Max iteration of two operators	100
c_2	Global acceleration coefficient (linearly increase from 0.5 to 2.5)	0.5–2.5	$Nc_{1\max}$	Max iteration of map and compass operator	75
w	Inertia weight (linearly decrease from 0.99 to 0.2)	0.99–0.2	$Nc_{2\max}$	Max iteration of landmark operator	25
D	Dimension of the search space for FOPID	10	D	Dimension of the search space for FOPID	10
N_{st}	Number of exploitation-subpopulation	70	N_{pt}	Number of exploitation-subpopulation	70
N_{sr}	Number of exploration-subpopulation	30	N_{pr}	Number of exploration-subpopulation	30
a_p	Learning probability coefficient	0.1	a_p	Learning probability coefficient	0.1
b_p	Learning probability coefficient	0.25	b_p	Learning probability coefficient	0.25

Table 3
Other parameters for simulations.

Parameter	Description	Value
V_T	Velocity of tanker	150 (m/s)
h	Height of AAR	7000 (m)
V_{R2T}	Velocity of receiver larger than V_T during approaching	1.5 (m/s)
d_{R2D}	Distance of receiver behind drogue	25 (m)
d_{pod}	Refueling pod's position relative to right wingtip	2.85 (m)
$(gust_u\ gust_v\ gust_w)$	Velocity of gust	(0 −3 2) (m/s)
$(d_x\ 0\ d_z)$	$O_vX_vY_vZ_v$ relative to tanker's body coordinate system	(2 0 2) (m)
h_{nose}	Maximum radius of fuselage width	0.4 (m)
U	Velocity of averaged flow	V_T (m/s)
b_T	Wingspan of tanker	39.88 (m)
m_T	Mass of tanker	120 000 (kg)
$(x_p\ y_p\ z_p)$	Probe's position relative to receiver's nose coordinate system	(−2.05 0.5 −0.86) (m)
b_f	Fitting coefficient	10
d_f	Fitting coefficient	9
$2M+1$	Order of fitting	7
$[\omega_1, \omega_2]$	Fitting frequency band	[0.35, 400]
$\boldsymbol{u}_0$	Opening angles of the drogue's equilibrium state	[30.24° 30.24° 30.24° 30.24°]
$\boldsymbol{C}_u$	Opening angular coefficients for aerodynamic force	$\begin{bmatrix} -8.64 & -10.41 & -8.64 & -3.44 \\ -56.4 & 0 & 56.4 & 0 \\ -3.44 & -53.4 & -3.44 & 53.0 \end{bmatrix} \times 10^{-4}$

h, velocity V_T, and the receiver starts to approach the drogue from $t = 50$ s until arrives at the drogue's initial stabilized position (i.e., the drogue's relative position at $t = 50$ s). Besides, the refueling pod is mounted around the right wingtip, and the initial states of HDS are $\vartheta_{k1} = 30°, \vartheta_{k2} = 0°, \dot{\vartheta}_{k1} = 0, \dot{\vartheta}_{k2} = 0$. In this case, the active-control of controllable drogue is not conducted.

The hose–drogue system simulation results for AAR docking in Case 1 are shown in Figs. 4–5. As illustrated in Fig. 4, the hose's simulation results effectively reflect the flexibility of hose which is susceptive to the multi-wind disturbances. As the assumptions in Case 1, in the first 50 s, the HDS stabilizes in the steady flow-field including the free stream and tanker trailing vortex as shown in Fig. 5(b), (c), (d). The initial stabilized position at the 50 s is listed in Table 4, which could be regarded as the target position in the following active-control for controllable drogue. When the multi-wind disturbances are added from the 50 s, the hose–drogue assembly starts to move from the initial stabilized position to the final swinging area as shown in Fig. 5(a). Noting that the capture radius was defined as 0.1 m [38] inside the outer ring of drogue, thus the effective capture radius is $R_c = 0.205$ m in this paper. In other words, if the drogue swings in the area of radius R_c, the receiver would successfully dock into the drogue in high probability. However, as we can see from Fig. 5(b), (c), (d) and Table 4, the max–min of drogue's position in three directions are respectively 0.184 m, 0.831 m, and 0.569 m much larger than $2R_c = 0.41$ m. Besides, the drogue has an obvious position offset at the 150 s comparing with the initial stabilized position. Since the high-frequency swing of the drogue, the receiver might be trapped into the problem of chasing the drogue, which could easily cause an accident.

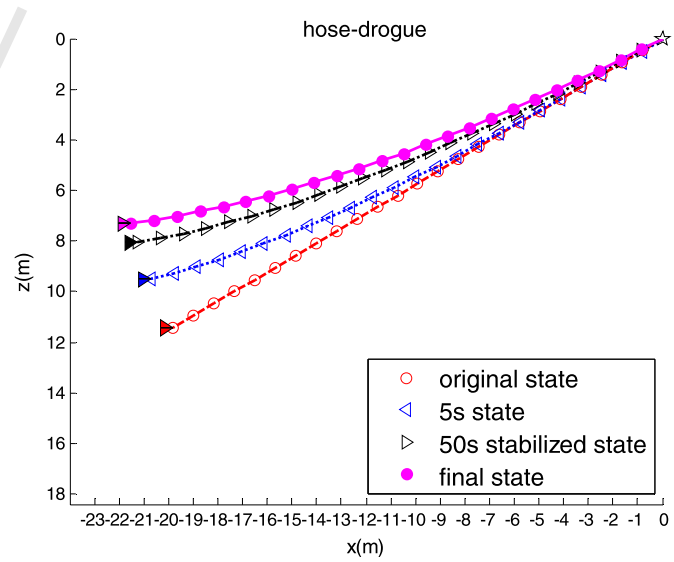

Fig. 4. States of hose–drogue system in Case 1.

UNCORRECTED PROOF

Please cite this article in press as: Y. Sun et al., Fractional-order controllers optimized via heterogeneous comprehensive learning pigeon-inspired optimization for autonomous aerial refueling hose–drogue system, Aerosp. Sci. Technol. (2018), https://doi.org/10.1016/j.ast.2018.07.034

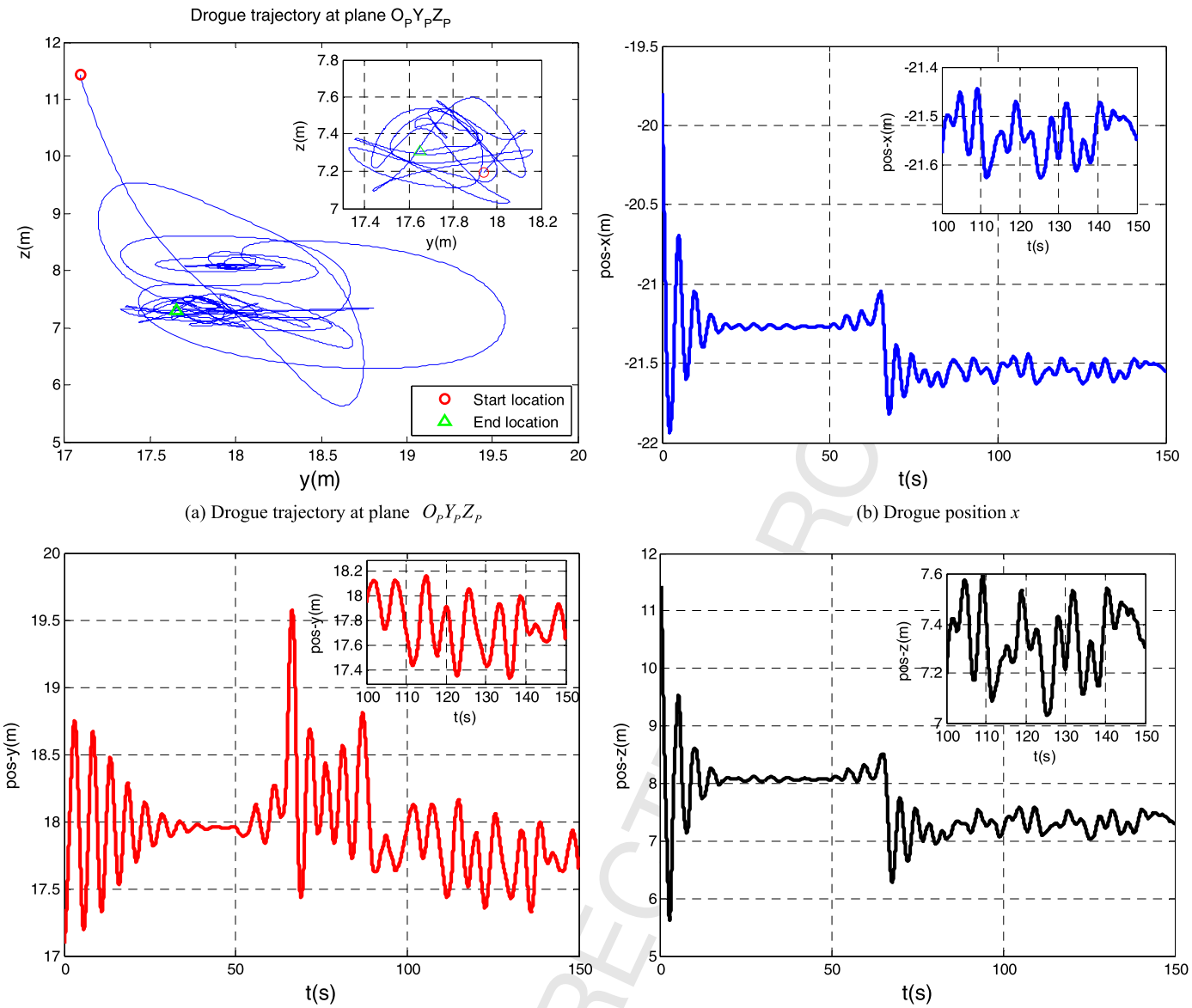

(a) Drogue trajectory at plane $O_PY_PZ_P$

(b) Drogue position x

(c) Drogue position y

(d) Drogue position z

Fig. 5. Simulation results for drogue position in Case 1.

Table 4
Drogue position statistical property (100–150 s).

		50 s	150 s	max–min	Mean	Variance
Without control	x (m)	−21.27	−21.55	0.184	−21.54	0.0020
	y (m)	17.961	17.652	0.831	17.769	0.0447
	z (m)	8.068	7.305	0.569	7.337	0.0181
Optimized PID	x (m)	−21.27	−21.30	0.048	−21.29	0.00011
	y (m)	17.961	17.922	0.138	17.960	0.00087
	z (m)	8.068	8.039	0.126	8.071	0.00077
Optimized FOPID	x (m)	−21.27	−21.28	0.026	−21.28	0.000036
	y (m)	17.961	17.944	0.049	17.960	0.00011
	z (m)	8.068	8.050	0.063	8.056	0.00018

Table 5
Parameters of the PID and FOPID controllers optimized by HCLPIO.

Controller	Parameters	Value
PID	$[k_P^s, k_I^s, k_D^s, k_P^v, k_I^v, k_D^v]$	[234.2184, 178.8385, 189.6352, 301.0738, 145.2843, 178.8409]
FOPID	$[k_P^s, k_I^s, k_D^s, \lambda^s, \mu^s, k_P^v, k_I^v, k_D^v, \lambda^v, \mu^v]$	[221.8123, 215.7172, 208.0687, 1.2719, 1.3176, 217.0255, 263.8515, 201.2188, 1.1983, 1.2897]

UNCORRECTED PROOF

Please cite this article in press as: Y. Sun et al., Fractional-order controllers optimized via heterogeneous comprehensive learning pigeon-inspired optimization for autonomous aerial refueling hose–drogue system, Aerosp. Sci. Technol. (2018), https://doi.org/10.1016/j.ast.2018.07.034

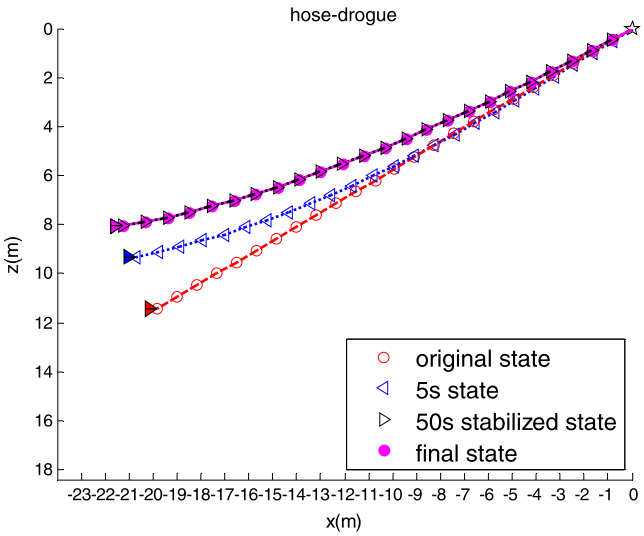

Fig. 6. States of hose–drogue system for FOPID controllers in Case 2.

Case 2. The assumptions of simulation are the same as Case 1. In this case, the optimized $PI^{\lambda}D^{\mu}$ and PID controllers for controllable drogue are respectively implemented from $t = 50$ s.

In Case 2, the optimized FOPID controllers are employed to stabilize the position of the controllable drogue, which certifies the FOPID controllers' validity. Implementing the design processes of the optimized controllers as identified in Section 4.2, assume that choose one of the four algorithms (PSO/PIO/HCLPSO/HCLPIO) successively for the FOPID controllers (as shown in Fig. 2), the parameters of FOPID controllers optimized via the four algorithms can be obtained. Similarly, assume that the controllers are chosen as the form of PID, we can acquire the parameters of PID controllers optimized via the four algorithms as well. Table 5 merely presents the parameters of PID and FOPID controllers optimized by HCLPIO. As shown in Fig. 6, the initial stabilized states of the hose–drogue assembly are extremely similar to the final states, which means the HDS commendably maintain the drogue's relative position via the optimized FOPID controllers. When compare Fig. 7(a) with Fig. 5(a), it can be concluded that the drogue stabilizes to a determinate relative position with minor swing because of the active-control aerodynamic forces generated by the control-

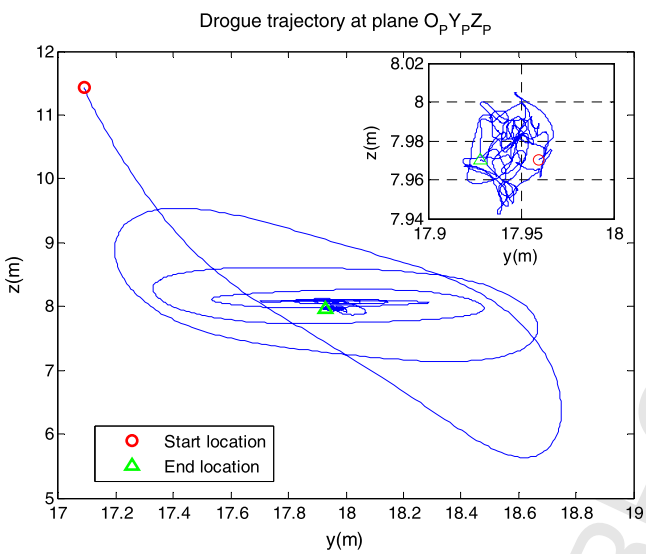

(a) Drogue trajectory at plane $O_PY_PZ_P$ for FOPID

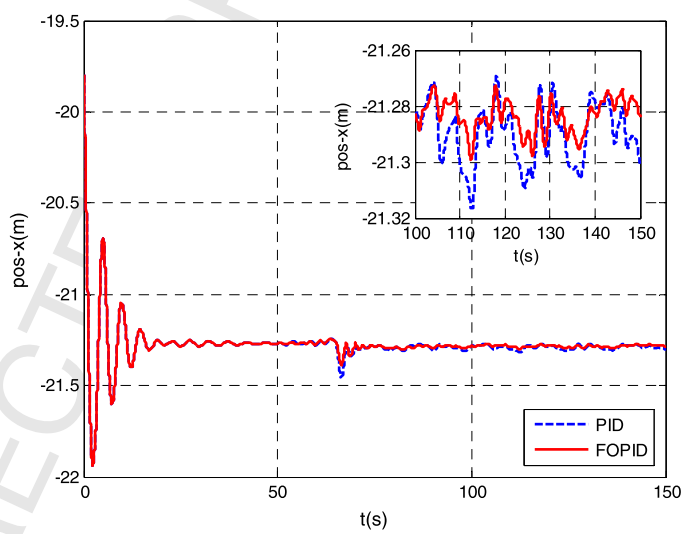

(b) Drogue position x for FOPID and PID

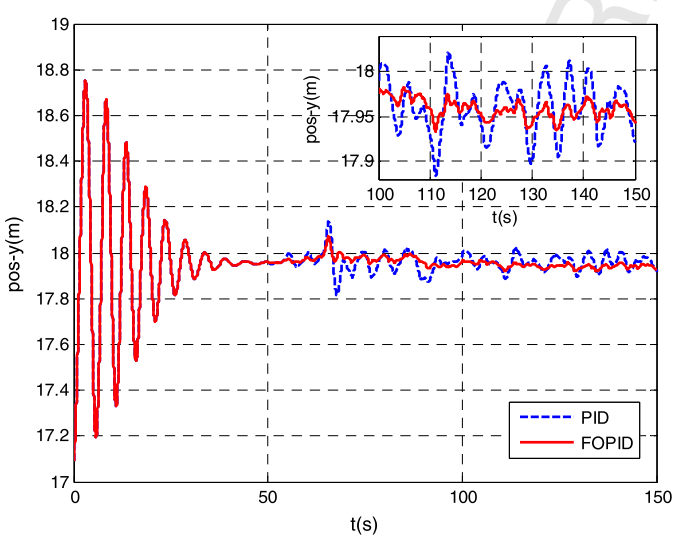

(c) Drogue position y for FOPID and PID

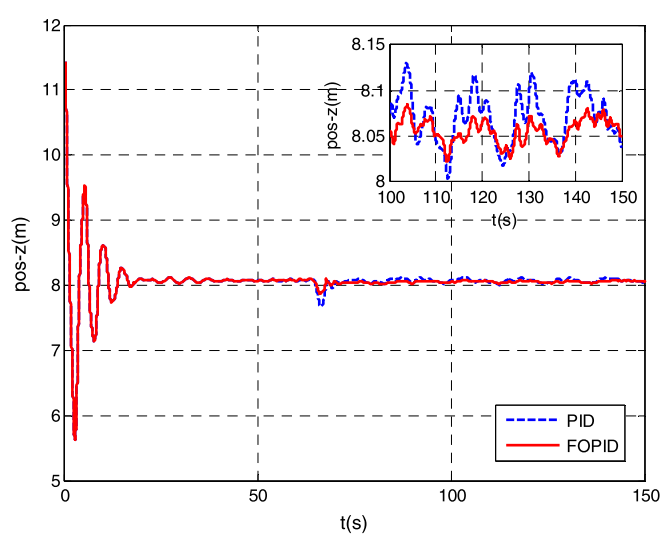

(d) Drogue position z for FOPID and PID

Fig. 7. Simulation results for drogue position in Case 2.

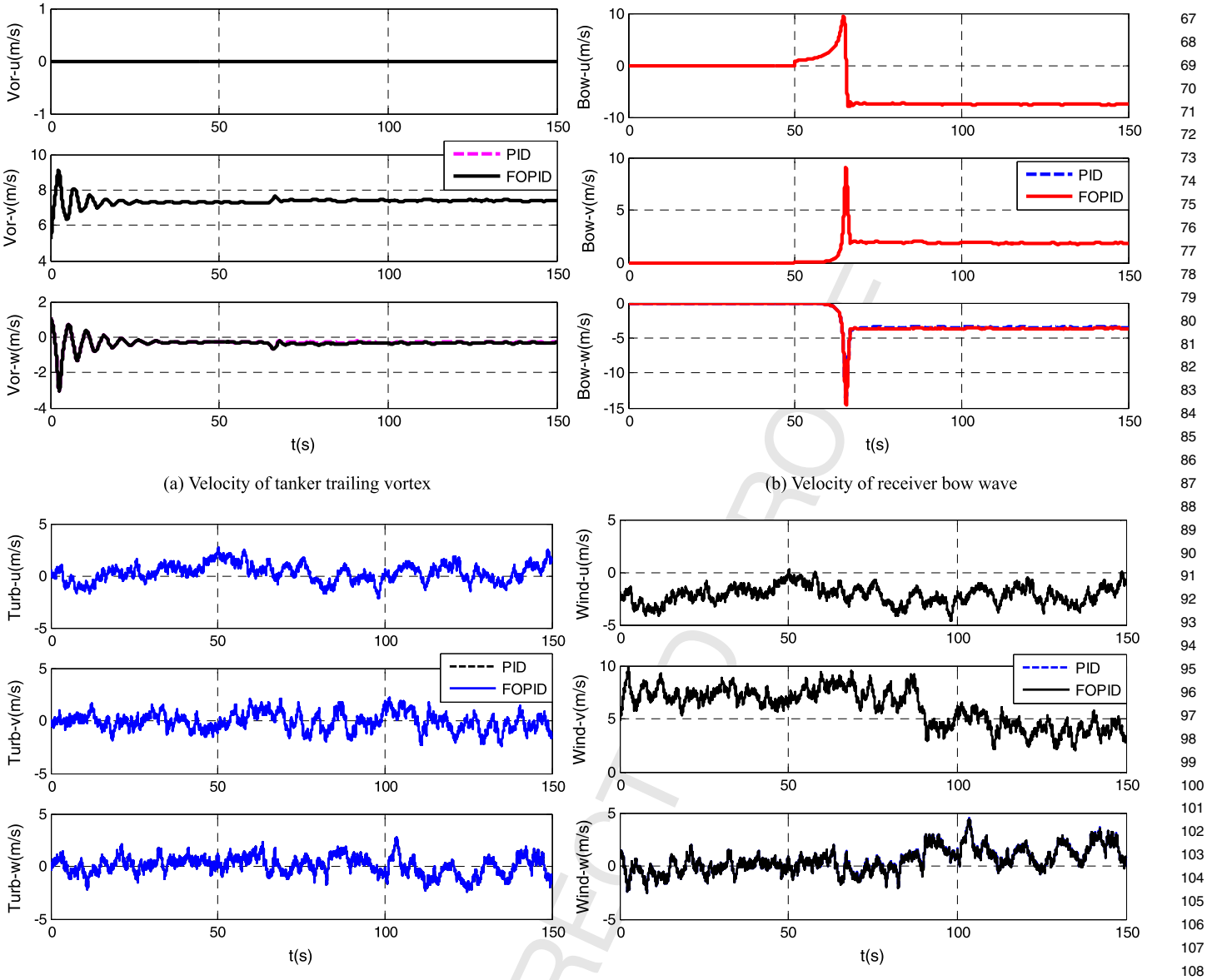

(a) Velocity of tanker trailing vortex

(b) Velocity of receiver bow wave

(c) Velocity of atmospheric turbulence

(d) Velocity of multi-wind disturbances

Fig. 8. Simulation results for multi-wind disturbances in Case 2.

lable drogue. Further, if the active-control for controllable drogue is off, as analyzed above, the swinging range of drogue does not meet the requirement of effective capture radius R_c. But when the FOPID controllers for controllable drogue is conducted, it can be seen from Fig. 7(b), (c), (d) that the drogue swings in a much smaller range than Case 1. Quantitatively, as listed in Table 4, there is an obvious reduction in the range of motion of the drogue's position: from 0.184 m to 0.026 m in x-axes, from 0.831 m to 0.049 m in y-axes, and from 0.569 m to 0.063 m in z-axes, which are within the range of $2R_c$. Besides, the variances of drogue's position for FOPID controllers are just a few hundredths of that without control at the 100–150 s. As shown in Fig. 8, due to the refueling pod mounted around the right wingtip, a relatively larger lateral wind velocity ($V'_{vory} \approx 7.5$ m/s) of the trailing vortex is generated, and the vertical wind velocity is approximate to zero. The wind velocity of the bow wave is denoted as $v_{bowy} > 0$, $v_{bowz} < 0$, which means the bow wave tends to push the drogue moving to the right top position. The atmospheric turbulence can be regarded as the high-frequency disturbance inducing the drogue's swing. Thus, it is essential that apply the optimized FOPID controllers to stabilize the drogue. From the results in Fig. 9, the active aerodynamic forces can be decomposed into two components: the stable component for resisting the trailing vortex, bow wave, gust, and wind shear; and the vibrating component for resisting the atmospheric turbulence. The role of active aerodynamic forces is equivalent to transform the unsteady flowfield to an approximate steady flowfield and compensate the influence of that. Further, as we can see from Fig. 10, the opening angles of actuators are deflected within a few degrees, which are limited in the normal range.

Additionally, the optimized PID controllers are adopted for the active-control of controllable drogue to further compare the optimized FOPID controllers. As indicated in Fig. 7(b), (c), (d), it is obvious that the optimized FOPID controllers perform superior than the optimized PID controllers for position stabilizing at the 100–150 s. We can clearly see from Table 4 that the variances of drogue's position for FOPID controllers in x, z-axes are merely about half of those for PID controllers, and the variance in y-axes is enhanced more significantly. Besides, comparing the drogue's position at the 150 s with that at the 50 s in Table 4, the steady-state offsets are smaller for FOPID controllers than the PID

UNCORRECTED PROOF

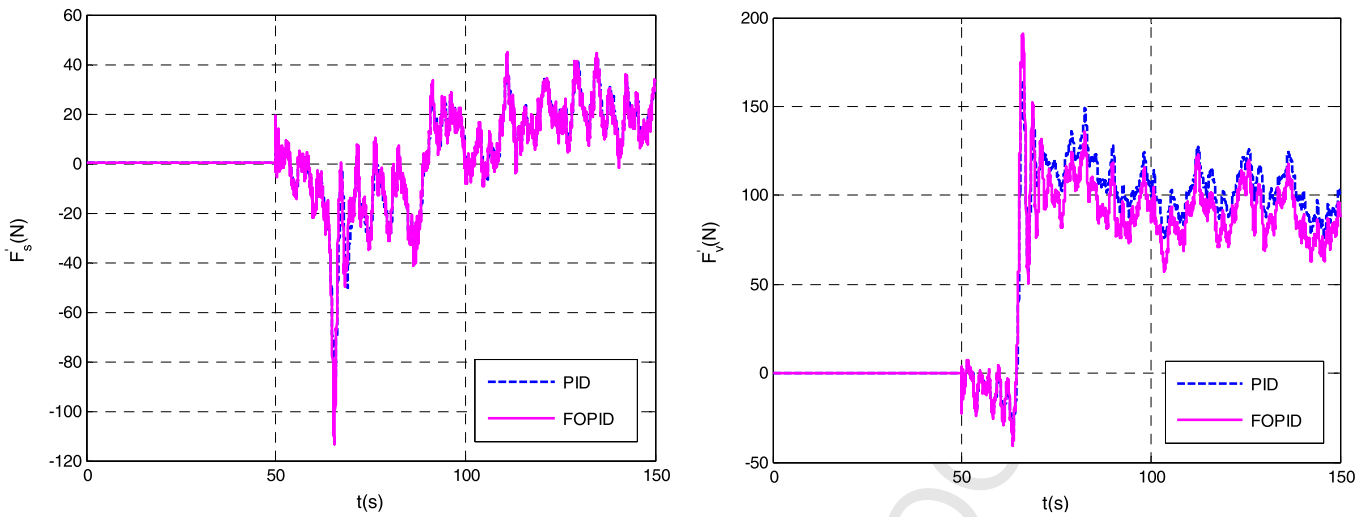

(a) Real lateral force (b) Real vertical force

Fig. 9. Simulation results for real lateral and vertical forces in Case 2.

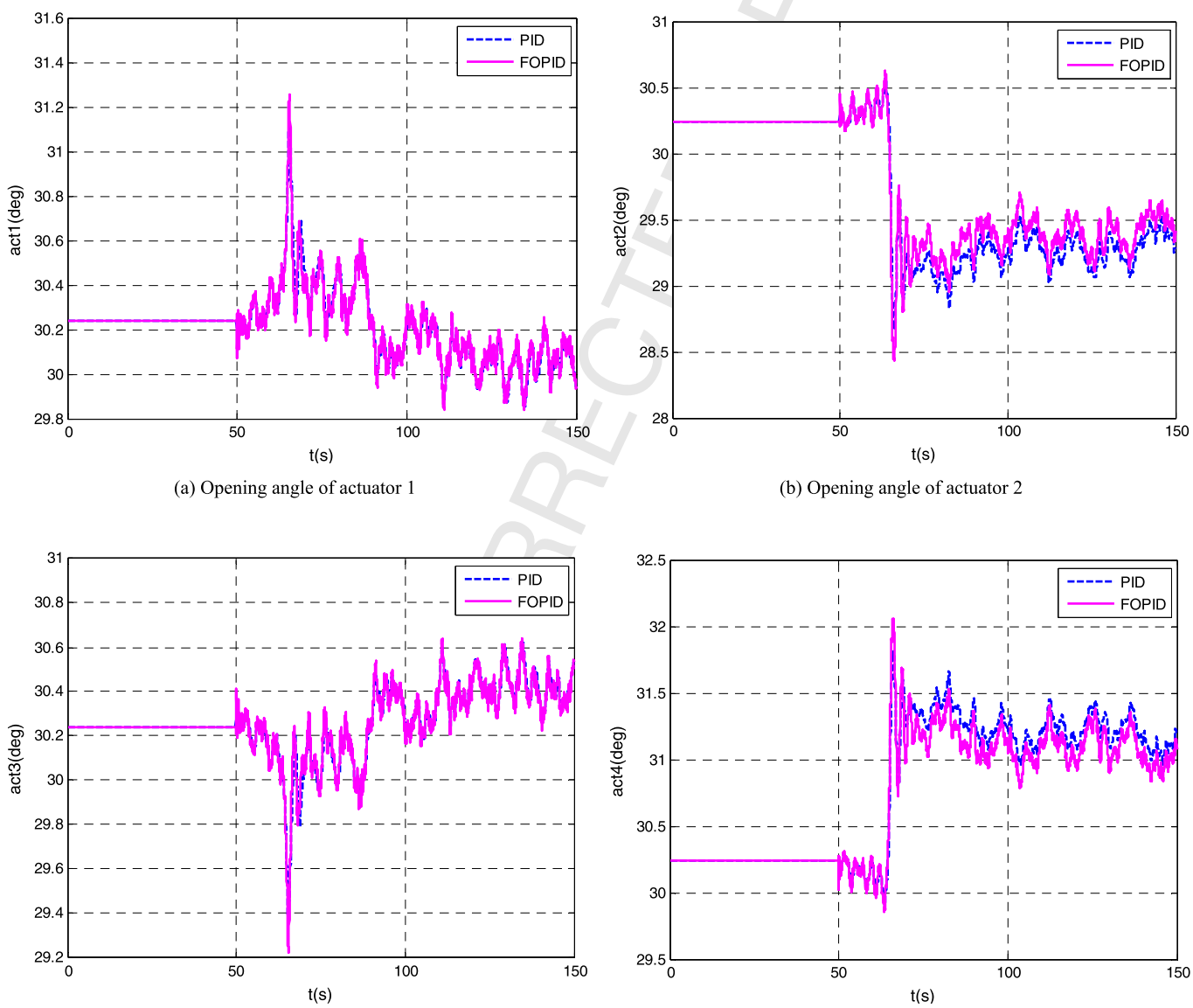

(a) Opening angle of actuator 1 (b) Opening angle of actuator 2

(c) Opening angle of actuator 3 (d) Opening angle of actuator 4

Fig. 10. Opening angles for actuators.

Please cite this article in press as: Y. Sun et al., Fractional-order controllers optimized via heterogeneous comprehensive learning pigeon-inspired optimization for autonomous aerial refueling hose–drogue system, Aerosp. Sci. Technol. (2018), https://doi.org/10.1016/j.ast.2018.07.034

Table 6
Comparative optimization results for FOPID controllers.

Algorithm	Controller parameters $[k_P^s, k_I^s, k_D^s, \lambda^s, \mu^s, k_P^v, k_I^v, k_D^v, \lambda^v, \mu^v]$	Fitness value
HCLPIO	[221.8123, 215.7172, 208.0687, 1.2719, 1.3176, 217.0255, 263.8515, 201.2188, 1.1983, 1.2897]	108.6358
PIO	[232.8871, 186.5465, 192.1504, 1.1855, 1.1100, 237.6300, 178.6573, 181.6861, 1.1698, 1.1844]	123.4095
HCLPSO	[242.1030, 170.4099, 228.2729, 1.4659, 1.2550, 252.8450, 241.7989, 214.0536, 1.1838, 1.3729]	119.1342
PSO	[199.2369, 198.4451, 183.6850, 1.0893, 1.1747, 197.5306, 246.6755, 192.9626, 1.0448, 1.1153]	127.3263

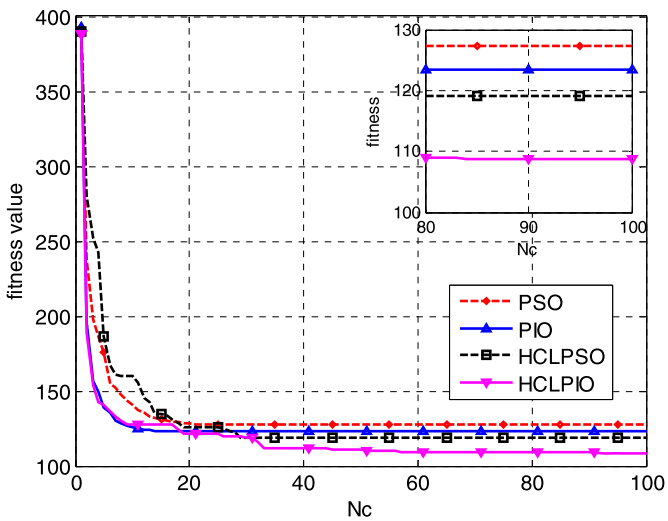

Fig. 11. Comparative evolution curves of four algorithms for FOPID controllers.

controllers. Therefore, as the comparative experiments mentioned above, the optimized FOPID controllers cannot merely stabilize the drogue's position in the presence of multi-wind disturbances, but also perform more efficiently than the optimized PID controllers.

To evaluate the effectiveness of our proposed HCLPIO, we respectively apply the four algorithms (PSO/PIO/HCLPSO/HCLPIO) to optimize the FOPID controllers in independent 10 runs and compare the average fitness values of different algorithms. As presented in Fig. 11 and Table 6, starting from the same initial fitness value, the proposed HCLPIO for the optimized FOPID controllers performs the best in terms of the fitness value, which means the HCLPIO optimized parameters possess the best capability for stabilizing the drogue's position. Besides, we also make some analysis about the tendency of the four algorithms' evolution curves for FOPID controllers as follows:

(1) It can be seen from Fig. 11 that the basic PIO converges faster than the basic PSO. The map and compass operator of PIO better refines the promising solutions in the entire search space to obtain the more optimal parameters for FOPID controllers.

(2) When compare HCLPIO, HCLPSO with basic PIO, PSO at the first 15 iterations, we draw a conclusion that the basic algorithms have a faster convergence rate than the modified version. Since the HCL strategy is introduced into the modified algorithms, the swarm populations are divided into two subpopulations, which reduces the convergence rate at the first few iterations.

(3) In turn, since the HCL strategy enhances the diversity of swarm populations at the late iterations, the HCLPIO is prevented to trap into the local optimal solutions. Thus, even at the late iterations, the HCLPIO still has stronger exploration capability to continuously update the pigeons for attaining the more optimal parameters.

6. Conclusions

In this paper, we design an optimized fractional-order PID controllers for stabilizing the position of drogue relative to the tanker. First, we investigate the dynamics of hose–drogue system, and model the hose–drogue assembly as a link-connected system based on the finite-segment multi-body method. Then, we establish the multi-wind disturbances environment including the tanker trailing vortex, receiver bow wave, atmospheric turbulence, gust, and wind shear for the HDS simulations in the docking stage of AAR. Moreover, a modified version of PIO, called HCLPIO, is proposed to enhance the diversity of swarm populations for the more optimal solution. Finally, the HCLPIO optimized FOPID controllers are designed to reduce the swinging range of controllable drogue for resisting the multi-wind disturbances. The simulation results indicate that our proposed optimized FOPID controllers for HDS are more effective than the optimized PID controllers for stabilizing the controllable drogue to swing within an acceptable range, and our proposed HCLPIO alleviates the workload on designers via optimizing the parameters of controllers. Our future work will emphasize on the application of our proposed approach for comprehensive simulations of AAR entire processes considering the control problems for tanker and receiver.

Conflict of interest statement

None declared.

Acknowledgements

This work was partially supported by Natural Science Foundation of China (NSFC) (Grant Nos. 61425008, 6133004, 91648205), Aeronautical Foundation of China (Grant No. 2015ZA51013).

Appendix A. Equations of PSO

The velocity $V_i(t)$ and position $X_i(t)$ of i-th particle at the t-th iteration are updated as follows:

$$V_i(t) = w \cdot V_i(t-1) + c_1 \cdot rand1_i \cdot \big(pbest_i - X_i(t-1)\big) + c_2 \cdot rand2_i \cdot \big(gbest - X_i(t-1)\big)$$

$$X_i(t) = X_i(t-1) + V_i(t-1)$$

where w denotes the inertia weight; c_1 and c_2 are acceleration coefficients; $rand1_i$ and $rand2_i$ represent the random numbers in the range of [0, 1]; $pbest_i$ is the best position of i-th particle; $gbest$ is the current global best position.

References

[1] P.R. Thomas, U. Bhandari, S. Bullock, et al., Advances in air to air refueling, Prog. Aerosp. Sci. 71 (2014) 14–35.
[2] J.A. Winnefeld, F. Kendall, FY2011-2036 unmanned system integrated roadmap, U.S. Department of Defense, 2011.
[3] P. Li, H.B. Duan, A potential game approach to multiple UAV cooperative search and surveillance, Aerosp. Sci. Technol. 68 (2017) 403–415.

[4] M. Radmanesh, M. Kumar, Flight formation of UAVs in presence of moving obstacles using fast-dynamic mixed integer linear programming, Aerosp. Sci. Technol. 50 (2016) 149–160.
[5] J.P. Nalepka, J.L. Hinchman, Automated aerial refueling: extending the effectiveness of unmanned air vehicles, in: AIAA Modeling and Simulation Technologies Conference and Exhibit, San Francisco, California, 2005, AIAA 2005-6005.
[6] Q. Quan, Z.B. Wei, J. Gao, et al., A survey on modeling and control problems for probe and drogue autonomous aerial refueling at docking stage, Acta Aeronaut. Astronaut. Sin. 35 (9) (2014) 2390–2410.
[7] E.F. Ward, S.A. Calif, Hose and Drogue Boom Refueling System, for Aircraft, USA, US5573206, 1996.
[8] M.J. Vachon, R.J. Ray, Calculated drag of an aerial refueling assembly through airplane performance analysis, in: 42nd AIAA Aerospace Sciences Meeting and Exhibit, Reno, Nevada, 2004, AIAA 2004-381.
[9] J.L. Hansen, J.E. Murray, N.V. Campos, The NASA Dryden Flight Test Approach to an Aerial Refueling System, NASA Dryden Flight Research Center, 2005, Report No.: NASA/TM-2005-212859.
[10] J.C. Vassberg, D.T. Yeh, A.J. Blair, et al., Dynamic characteristics of a KC-10 wing-pod refueling hose by numerical simulation, in: 20th Applied Aerodynamics Conference, St. Louis, Missouri, 2002, AIAA 2002-2712.
[11] Z.H. Zhu, S.A. Meguid, Modeling and simulation of aerial refueling by finite element method, Int. J. Solids Struct. 44 (2007) 8057–8073.
[12] K. Ro, J.W. Kamman, Modeling and simulation of hose–paradrogue aerial refueling systems, J. Guid. Control Dyn. 33 (1) (2010) 53–63.
[13] W.R. Williamson, G.J. Glenn, S.M. Stecko, et al., Controllable drogue for automated aerial refueling, J. Aircr. 47 (2) (2010) 515–527.
[14] H.T. Wang, X.M. Dong, J.P. Xue, et al., Dynamic modeling of a hose–drogue aerial refueling system and integral sliding mode backstepping control for the hose whipping phenomenon, Chin. J. Aeronaut. 27 (4) (2014) 930–946.
[15] K. Ro, T. Kuk, J.W. Kamman, Active control of aerial refueling hose–drogue systems, in: AIAA Guidance, and Control Conference, Toronto, Ontario Canada, 2010, AIAA 2010-8400.
[16] S.C. Kriel, J.A.A. Engelbrecht, T. Jones, Receptacle normal position control for automated aerial refueling, Aerosp. Sci. Technol. 29 (1) (2013) 296–304.
[17] P.R. Thmoas, S. Bullock, T.S. Richardson, et al., Collaborative control in a flying-boom aerial refueling simulation, J. Guid. Control Dyn. 38 (7) (2015) 1274–1289.
[18] J.Y. Cao, B.G. Cao, Design of fractional order controller based on particle swarm optimization, Int. J. Control. Autom. Syst. 4 (6) (2006) 775–781.
[19] B. Shang, J.X. Liu, T.B. Zhao, et al., Fractional order robust visual serving control of a quadrotor UAV with larger sampling period, in: 2016 International Conference on Unmanned Aircraft Systems, 2016, pp. 1228–1234.
[20] C.H. Im, H.K. Jung, Y.J. Kim, Hybrid genetic algorithm for electromagnetic topology optimization, IEEE Trans. Magn. 39 (5) (2002) 2163–2169.
[21] P. Riccardo, J. Kennedy, T. Blackwell, Particle swarm optimization, Swarm Intell. 1 (1) (2007) 33–57.
[22] D. Karaboga, B. Basturk, A powerful and efficient algorithm for numerical function optimization: artificial bee colony (ABC) algorithm, J. Glob. Optim. 39 (3) (2007) 459–471.
[23] J.N. Li, H.B. Duan, Simplified brain storm optimization approach to control parameter optimization in F/A-18 automatic carrier landing system, Aerosp. Sci. Technol. 42 (2015) 187–195.
[24] W.R. Zhu, H.B. Duan, Chaotic predator-prey biogeography-based optimization approach for UCAV path planning, Aerosp. Sci. Technol. 32 (1) (2014) 153–161.
[25] H.B. Duan, X.X. Wei, Z.N. Dong, Multiple UCAVs cooperative air combat simulation platform based PSO, ACO, and game theory, IEEE Aerosp. Electron. Syst. Mag. 28 (11) (2013) 12–19.
[26] H.B. Duan, P.X. Qiao, Pigeon-inspired optimization: a new swarm intelligence optimizer for air robot path planning, Int. J. Intell. Comput. Cybern. 7 (1) (2014) 24–37.
[27] C. Li, H.B. Duan, Target detection approach for UAVs via improved pigeon-inspired optimization and edge potential function, Aerosp. Sci. Technol. 39 (2014) 352–360.
[28] S.J. Zhang, H.B. Duan, Gaussian pigeon-inspired optimization approach to orbital spacecraft formation reconfiguration, Chin. J. Aeronaut. 28 (1) (2015) 200–205.
[29] G. Sushnigdha, A. Joshi, Re-entry trajectory design using pigeon inspired optimization, in: AIAA Atmospheric Flight Mechanics Conference, Denver, Colorado, 2017, AIAA 2017-4209.
[30] J. Zhao, R. Zhou, Pigeon-inspired optimization applied to constrained gliding trajectories, Nonlinear Dyn. 82 (4) (2015) 1781–1795.
[31] N. Lynn, P.N. Suganthan, Heterogeneous comprehensive learning particle swarm optimization with enhanced exploration and exploitation, Swarm Evol. Comput. 24 (2015) 11–24.
[32] S. Venkataramanan, A. Dogan, Modeling of aerodynamic coupling between aircraft in close proximities, in: AIAA Atmospheric Flight Mechanics Conference and Exhibit, Providence, Rhode Island, 2004, AIAA-2004-5172.
[33] U. Bhandari, P.R. Thomas, S. Bullock, et al., Bow wave effect in probe and drogue aerial refuelling, in: AIAA Guidance, Navigation, and Control (GNC) Conference, Boston, MA, 2013, AIAA-2013-4695.
[34] S. Gage, Creating a unified graphical wind turbulence model from multiple specifications, in: AIAA Modeling and Simulation Technologies Conference and éExhibit, Austin, Texas, 2003, AIAA 2003-5529.
[35] V. Feliu-Batle, R.R. Pérez, L.S. Rodríguez, Fractional robust control of main irrigation canals with variable dynamic parameters, Control Eng. Pract. 15 (2007) 673–686.
[36] S.M. Wang, H. Wang, Design and simulation of fractional order PID controller, Modern Def. Technol. 43 (6) (2015) 204–208.
[37] I. Podlubny, I. Petráš, B.M. Vinagre, et al., Analogue realizations of fractional-order controllers, Nonlinear Dyn. 29 (1–4) (2002) 281–296.
[38] R.P. Dibley, M.J. Allen, Autonomous airborne refueling demonstration phase I flight-test results, in: AIAA Atmospheric Flight Mechanics Conference and Exhibit, Hilton Head, South Carolina, 2007, AIAA 2007-6639.
[39] J.C. Vassberg, D.T. Yeh, A.J. Blair, et al., Numerical simulation of KC-10 wing-mount aerial refueling hose–drogue dynamics with a reel take-up system, in: 21st Applied Aerodynamics Conference, Orlando, Florida, 2003, AIAA 2003-3508.

UNCORRECTED PROOF

Please cite this article in press as: Y. Sun et al., Fractional-order controllers optimized via heterogeneous comprehensive learning pigeon-inspired optimization for autonomous aerial refueling hose–drogue system, Aerosp. Sci. Technol. (2018), https://doi.org/10.1016/j.ast.2018.07.034